Comparison of Flame Describing Functions Measured in Single and Multiple Injector Configurations

Preethi Rajendram Soundararajan, D. Durox, Guillaume Vignat, Antoine Renaud, Jérôme Beaunier, Sébastien Candel

GTP-22-1360

Comparison of flame describing functions measured in single and multiple injector configurations

Preethi Rajendram Soundararajan [1]*, Daniel Durox [1], Guillaume Vignat [1], Antoine Renaud [1], Jérôme Beaunier [1], Sébastien Candel [1]

[1]Laboratoire EM2C, CNRS, CentraleSupélec, Université Paris-Saclay, 3, rue Joliot Curie, 91192 Gif-sur-Yvette cedex, France

ABSTRACT

Recent investigations of combustion instabilities in annular systems indicate that considerable insights may be gained by using information gathered in single-sector experiments. Such experiments are, for example, employed to measure flame describing functions (FDFs), which represent the flame response to incident perturbations. These data may be used in combination with low-order models to interpret instabilities in multiple injector annular systems. It is known, however, that the structure and dynamical behavior of an isolated flame do not necessarily coincide with those of a flame placed in an annular environment with neighboring side flames. It is then worth analyzing effects that may be induced by the difference in lateral boundary conditions and specifically examining the extent to which the FDF data from single-sector experiments portrays the dynamical response of the flame in the annular environment. These issues are investigated with a new setup, named TICCA-Spray, that comprises a linear arrangement of three injectors. The central flame is surrounded by two identical side flames in a rectangular geometry with key dimensions, side-wall separation, and spacing between injectors identical to those of the annular system MICCA-Spray. The describing function of the central flame is determined with techniques recently developed in single-sector experiments (SICCA-Spray). The FDFs obtained in the two configurations are compared for two swirler types having different swirl numbers and pressure drops. The effect of the swirl direction of the neighboring injectors is also explored by operating with co- and counter-swirl combinations. Differences between FDFs determined in the two test facilities, sometimes modest and in other cases less negligible, are found to depend on

*Address all correspondence to this author.

the flames' spatial extension and interactions. The general inference is that the FDFs measured in a single-injector combustor are better suited if the flame-wall interaction is weak, and provided that the area is equivalent to that of a single sector of an annular combustor. Nonetheless, using a multi-injector system would be more appropriate for a more precise FDF determination.

Keywords: Flame describing function; Swirling injector; Multiple-injector combustor; Spray flames.

NOMENCLATURE

MICCA-Spray	Sixteen-injector annular combustor
SICCA-Spray	Single-injector cylindrical test rig
TICCA-Spray	Three-injector linear test rig
A_I	Injection surface area
A_{BP}	Backplane surface area
s_I/d_I	Spacing to diameter ratio
707, 716	Clockwise swirlers
807, 816	Anticlockwise swirlers
d_{sc}	Swirler channel diameter
$R_{0,sc}$	Swirler channel radial location
S	Swirl number
ΔP	Pressure drop
σ	Head loss coefficient
u_b	Bulk velocity
F1, F2	Operating points
ϕ	Equivalence ratio
P_{th}	Thermal power
$\dot{Q}$	Heat release rate (HRR)
$\dot{q}_v$	Volume flow rate
$(.)'$	Root mean square fluctuations
$\overline{(.)}$	Mean
$\mathcal{F}$	Flame describing function (FDF)
$u_{c,r}$	Axial velocity at the injector exit
ω	Angular frequency such that $\omega = 2\pi f$, where f is the frequency
G	Gain of flame describing function

φ	Phase of flame describing function
γ^2	Signal coherence
S_{xx}	Power spectral density of signal x
S_{xy}	Cross power spectral density between input signal x and output signal y
V_0	Amplifier voltage

1 INTRODUCTION

Controlling combustion instabilities in annular systems is still a challenge, especially in systems operating in the lean premixed mode in compact, weakly-damped geometries. These instabilities are caused by a coupling between the acoustics of the system and the dynamics of the flames. The acoustic modes can be longitudinal or, more often, azimuthal, corresponding to the largest dimension of the annular chamber and consequently to the lowest frequencies where flames are most sensitive to disturbances. These instabilities are sustained by oscillations in the heat release rate (HRR) of the flames formed by the injection units [1–9]. It is generally considered that the transverse velocities that accompany azimuthal modes contribute to a lesser extent to the process, but some recent experiments indicate that when the oscillation level reaches large amplitudes, these velocities may extinguish flames located near the pressure nodal line [10]. In an annular combustor, if the flame dynamics are mainly driven by axial disturbances and well defined by the flow fluctuations in each injector [4, 11], and if the damping rate of the system can be estimated, it is possible to determine the amplitude of the limit cycle and infer the nature of the azimuthal oscillation (standing or spinning) that prevails in the system as exemplified in [12].

The analysis of these instabilities is usually based on low-order models accounting for the flame response to acoustic modulations in combination with a proper description of the injector dynamics and system acoustics [13]. The flame response is conveniently represented by the flame describing function (FDF) [14] or at least by a flame transfer function (FTF). In general, the FDF is measured separately on a single-injector configuration equipped with an acoustic flow modulation system to obtain the stable flame response. Transfer or describing function concepts suitably represent the complex multidimensional dynamics of real flames if the combustion region is compact with respect to the wavelength and interactions between flames are weak. One must also make sure that the FDF measured in a single-injector setup reliably describes the flame response and that this knowledge can be transposed to the annular configuration.

For dynamical similarity, it is generally believed that the confinement ratio, *i.e.*, the ratio of the injection surface area to the backplane surface area A_I/A_{BP}, should take identical values in the single-sector and annular configurations. This alone, however, may be inadequate because there is a notable difference in boundary conditions: a rigid wall cannot properly reflect possible interactions between adjacent flames. Even if the interactions between the neighboring flames appear to be weak [4,5,11], there is evidence that the proximity and arrangement of injection units (co- or counter-rotating) may influence the dynamics of the annular combustor [6, 15]. In addition, the flames are generally swirling, causing a strong rotation of the burnt gases between the flames. These effects may be enhanced if the injectors are fitted with an outlet cup [16, 17].

Several investigations carried out in linear geometries comprising a few swirling injectors indicate that relative injector

positions (represented by the spacing to diameter ratio s_I/d_I) and flame shapes determine the level of interactions between neighboring flames [18–20]. If the flames are in close proximity and expanding sideways, strong interactions can take place between the reactive layers, with significant variations in the instantaneous heat release rate [15, 21–23]. In [23], it is shown in particular that two close flames do not have the same FTF as an isolated flame. Differences have been observed not just in the dynamical response of the flame but also in the lean blow-off limits, as indicated in a recent study [24] conducted with a multi-burner linear combustor. One is led to think that the flame dynamics in an annular system will differ from the dynamics of a flame in a single-sector, even if the flame fronts are not in direct contact. This aspect was already considered in the past in [25–27]. Additionally, the problem of assigning a surface area to the single-injector backplane was also discussed in [26]. It was found that to avoid interactions between the flame and wall in the single-sector configuration and to obtain a flame shape that matches with that found in the annular multiple injector system, the cross-sectional area of the single-injector combustor $A_{BP}|_{\mathrm{SIC}}$ has to be a few times that of a single segment in the annular chamber $A_{BP}|_{\mathrm{AC}}$, depending on the swirl number. However, such a large distortion in the surface area ratio A_I/A_{BP} might not guarantee similar flame dynamics in the single-injector geometry and in the annular combustor. Smith *et al.* [27] also consider the difference in flow and flame behaviors between single- and multi-injector configurations, but in contrast with what was initially expected, they find no significant changes in flame dynamics. However, this study was carried out at a single frequency, and the flames were only subjected to transverse acoustic modulations. Recent investigations carried out at the EM2C laboratory [28] indicate that FDFs measured in a single-injector cylindrical combustor (SICCA-Spray) having the same area as one segment of an annular combustion chamber (MICCA-Spray) can be used to analyze and approximately predict the instabilities observed in the annular combustor. However, it is also noted that the flame dynamics in the single-injector arrangement does not completely match that prevailing in the annular chamber.

Previous studies do not consistently conclude whether a single-injector configuration would sufficiently represent an annular combustor with multiple injectors. It is clearly important to investigate these issues in further detail and specifically aim at comparing the FDFs obtained in single-sector and multiple-sector systems. The choice is made to conserve the same ratio between the injector outlet surface area and the backplane surface area A_I/A_{BP}, relative spacing s_I/d_I, and injector diameter in the single-sector and multiple-injector systems. A new test bench (designated as TICCA-Spray) was designed to complement the existing single-injector (SICCA-Spray) and annular combustor MICCA-Spray. TICCA-Spray comprises a set of three injectors in a rectangular geometry. The central flame is surrounded by two side flames in a geometry that portrays in a linear fashion the situation that prevails in the annular system.

This new experimental bench is described in Section 2, which also briefly discusses the related facilities: SICCA-Spray and MICCA-Spray. Section 3 is concerned with the flame describing function formulation and the treatment of the present spray flames as a single input single output (SISO) system. Data gathered in this new facility are presented in Section 4 and finally compared in Section 5 with FDFs determined with the single-injector configuration.

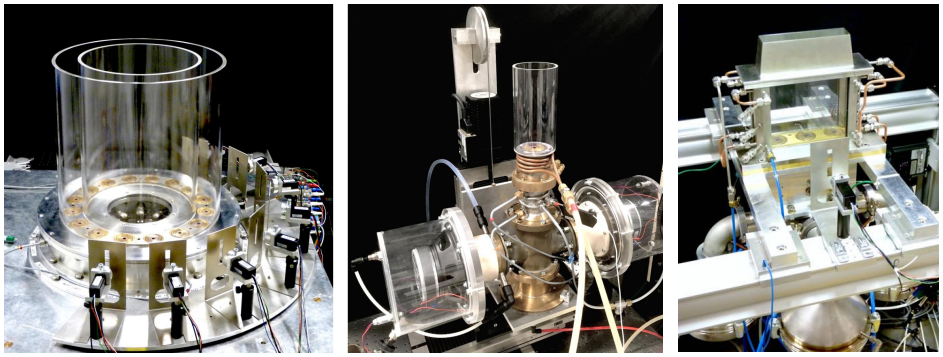

(a) MICCA-Spray (b) SICCA-Spray (c) TICCA-Spray

Fig. 1: (a) Photograph of the MICCA-Spray test rig. The mean diameter of the chamber is 350 mm and the walls are 400 mm long. (b) View of the SICCA-Spray test rig. The cylindrical flame tube has a 69 mm inner diameter and is 200 mm long. (c) The linear combustor, namely TICCA-Spray, equipped with three injectors. Acoustic actuators mounted inside metal enclosures are visible at the bottom of the photograph. A photomultiplier (in black) is installed in front of the quartz window, behind a mask with a vertical rectangular slot serving as a spatial filter.

2 EXPERIMENTAL SETUP

It is natural to begin by briefly describing the MICCA-Spray annular combustor shown in Fig. 1 (a) since it forms the basis of the geometrical configurations for SICCA-Spray and TICCA-Spray. This system is presented in further detail in [28]. It is equipped with sixteen swirl-spray injectors and is now mainly fed with liquid heptane or dodecane. It may also be operated with a premixed flow of air and propane. The chamber is made of transparent quartz walls open to the atmosphere. The inner and outer diameters of the annulus are 300 and 400 mm, respectively. Strong azimuthal instabilities were first observed with a 200 mm long inner tube and an outer tube 600 mm long [10] or 700 mm long [29], but in recent studies [28], strong and persistent azimuthal instabilities were recorded with lateral tubes of equal length (400 mm). The instabilities of MICCA-Spray have until now been interpreted using FDFs measured in the single-injector facility, SICCA-Spray. This configuration is shown in Fig. 1(b) and described in detail in [30]. The inner diameter of the flame tube is 69 mm, which corresponds to the area of a single sector of the annular chamber. For FDF measurements, the flame tube is sufficiently short, with a typical length of 150 mm, to avoid any longitudinal instabilities. Two driver units confined in cylindrical enclosures serve to oscillate the air flow at the injector outlet.

The same injector unit is used in MICCA-spray and SICCA-spray rigs, and its exploded view is shown in Fig. 2. Liquid heptane is delivered by an axial manifold to the hollow cone atomizer, which then sprays the fuel into the combustion chamber in the form of fine droplets. The air distributor delivers air around the atomizer to the six channels of the radial swirler. The geometrical parameters d_{sc} representing the swirler hole diameter and $R_{0,sc}$ representing the distance between the axis of the hole and the axis of the swirler can be suitably modified to obtain different swirl numbers and pressure drops. The injector assembly contains a terminal plate at its end, which has a conical hole of 8 mm outlet diameter. Two distinct swirlers, designated as 707 and 716, having different swirl numbers and pressure drops, are investigated in what follows. These swirlers produce a clockwise rotation of the air flow, and their parameters are tabulated in Tab. 1. In addition, the counterclockwise version of the two swirlers, designated as 807 and 816, having identical geometries as their clockwise counterpart, are also investigated. It is pointed out that, in SICCA-Spray, the clockwise and counterclockwise counterparts

Table 1: Injector characteristics obtained under cold flow conditions in SICCA-Spray. Δp represents the pressure drop of the injector and S designates the experimentally obtained swirl number. The head loss coefficient σ is calculated using the equation $\Delta p = \frac{1}{2}\sigma\rho_0 u_b^2$, where u_b is the bulk velocity given by $\dot{m}_{\text{air}}/\pi\rho_0 R_{\text{inj}}^2$ and $R_{\text{inj}} = 4\,\text{mm}$. d_{sc} is the diameter of the swirler channels and $R_{0,sc}$ is the distance between the axis of the hole and the axis of the swirler as shown in Fig. 2. F1 and F2 refer to the operating points defined in Tab. 2. Adapted from [30].

Swirler	S	Δp		σ	d_{sc}	$R_{0,sc}$
	(-)	(kPa)		(-)	(mm)	(mm)
		F1	F2			
707/807	0.60	3.65	2.81	3.30	4.0	4.6
716/816	0.70	5.74	4.41	5.20	3.5	4.7

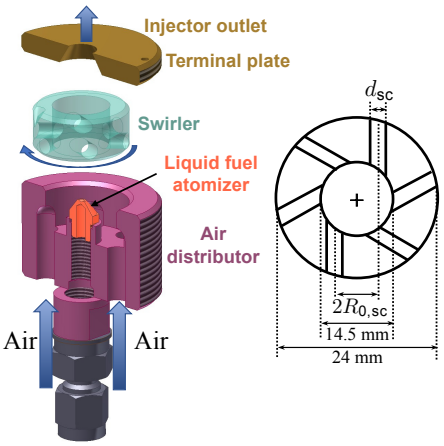

Fig. 2: The injector unit comprises an air distributor, a hollow cone atomizer, a swirler, and a terminal plate. The terminal plate features a converging conical shape having a diameter of 8 mm at the outlet. The schematic of the swirler is shown on the right. The channel diameter d_{sc} and radial location $R_{0,sc}$ can be varied to modify the swirl number and pressure drop.

cannot be distinguished as they possess the same characteristics.

The newly built TICCA-Spray linear combustor is shown in Fig. 1 (c). It comprises an array of three injectors, identical to those used in MICCA-Spray and SICCA-Spray, with a spacing of 69 mm between injectors. The choice of a system featuring three injectors is made so that the configuration remains simple enough but allows studying the effect of lateral boundary conditions on the flame dynamics. This is suitable as shown in [17], where it is found that the flow fields around the central injector in arrays with three or five injectors are quite close, provided that the spacing between injectors is kept constant. The combustion chamber is formed by four transparent windows that have a length of 205 mm, a width of 50 mm, and a height of 175 mm. The width is equal to the distance between the two sidewalls in MICCA-Spray and the length to the curvilinear distance corresponding to three adjacent injectors in MICCA-Spray. The height of TICCA-Spray is chosen such that the flames are stable and also sufficiently confined as in the annular chamber. The central flame in the linear array is, therefore, in a configuration close to that of the annular chamber, with neighboring swirling flames on each side. A slightly converging metallic hat placed on top of the transparent chamber prevents the entrainment of outside air and its inflow into the chamber. The backplane and the metallic corner structures supporting the lateral windows are cooled by circulating cold water. A sectional view passing through the axis of the central injector and perpendicular to the length of the

Table 2: Operating conditions considered in this study. ϕ is the global equivalence ratio and u_b is the mean air flow velocity per injector at the outlet.

Operating point (-)	ϕ (-)	u_b (/injector) ($\mathrm{m\,s^{-1}}$)	P_{th} SICCA (kW)	P_{th} TICCA (kW)
F1	0.85	42.7	6.4	19.3
F2	0.95	37.7		

chamber is shown in Fig. 3. The driver units for modulating the air flow are mounted inside metal enclosures and connected through elbow channels to the common air manifold (see Fig. 1 (c)). These are Monacor SP-6/108PRO hi-fi speakers with a root mean square power rating of 100 W and an electrical impedance of 8 Ω, capable of operating in the frequency range between 44 to 4500 Hz. The driver units modulate the air flow longitudinally along the axis of the injectors. In this study, each injector is supplied with liquid heptane as fuel delivered by a central axial tube passing through the plenum. The total air flow rate is controlled by a Bronkhorst EL-FLOW® mass flow meter of $500\mathrm{l_n/min}$, and the liquid fuel is controlled by a Bronkhorst CORI-FLOW™ mass flow meter with a full-scale of $10\,\mathrm{kg\,h^{-1}}$. Both the air and fuel are supplied under ambient temperature. The FDF measurements in TICCA-Spray are carried out on the central flame and compared with FDFs determined in SICCA-Spray at two operating conditions defined in Tab. 2. These operating points, designated as F1 and F2, correspond to the same thermal power but differ in the global equivalence ratio ϕ. While F2 is close to stoichiometry ($\phi = 0.95$), F1 is leaner ($\phi = 0.85$).

The test rig is equipped with a Hamamatsu type H11902-110 photomultiplier (PM) with an OH^* filter centered at 308 nm. A mask is placed in front of the PM such that it only collects the light emitted by the central flame (see Fig. 1 (c)). In a previous study carried out with the same type of injectors [30], the spray flames considered here did not show any significant spatial inhomogeneities of equivalence ratio during flow modulation in the frequency range of interest. This is because a large part of the spray is directed towards the conical wall of the terminal plate (see Fig. 2) before exiting into the chamber. This part of the fuel would then be approximately modulated in phase with the air pulsations. It might also be possible that the droplets interacting with the wall will slide along or bounce back and be swept away by the pulsating air flow. It is difficult to exactly identify the interaction mechanism, but whatever the scenario, it has been shown in [30] that the fluctuation of the overall equivalence ratio (or mixture ratio) at the injector outlet is relatively weak compared to the fluctuation in velocity. This is deduced from measurements of the ratio $I(CH^*)/I(OH^*)$ and images of this ratio in the flame at various instances during the oscillation cycle. It is known that this ratio can be linked to the equivalence ratio in the flame, and the relation may be calibrated by making use of measurements under steady conditions. It is found that the relative global equivalence ratio fluctuation is 4% at 500 Hz, which is relatively small compared to the relative velocity fluctuation of 22% at this frequency. Other experiments (presented in [30]) indicate that fluctuations in $I(CH^*)/I(OH^*)$ are of the same order of magnitude when the injector is fed with a fully premixed stream of propane and air or when it is fed with liquid heptane and air. One may thus consider that the spray flames investigated in the present experiments behave like premixed

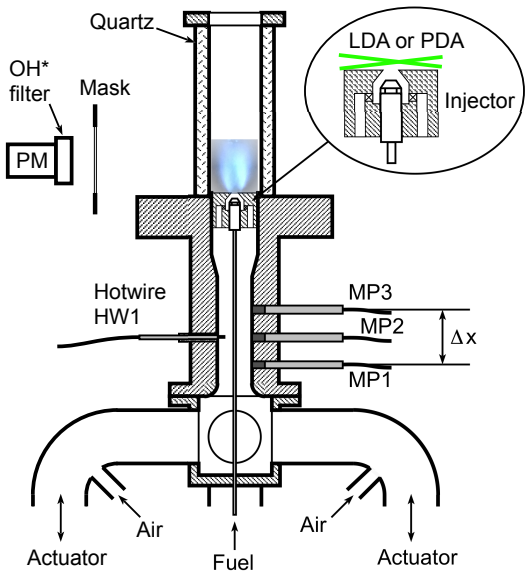

Fig. 3: Sectional view of the TICCA-Spray combustor in a plane perpendicular to the length and passing through the central burner axis.

flames, that their chemiluminescence characteristics are similar to those of premixed flames [31, 32], and that the OH^* light emission may serve as an acceptable indicator of the HRR.

The velocity in the chamber is measured with a Dantec Dynamics FlowExplorer 2-component phase Doppler anemometer (PDA), which is also used to measure droplet size in the spray. For velocity measurements, the system is configured in laser Doppler anemometry mode (LDA) to augment the data rate compared to the PDA mode. Further details of the PDA/LDA system are provided in [30]. The size of the spray droplets at the location of velocity measurements does not exceed a mean diameter of 5 µm, resulting in low inertia for the droplets in the air flow. At an oscillation frequency of 500 Hz, a standard calculation indicates that the amplitude of the droplet velocity fluctuation is 0.95 that of the local velocity of the gas and that there is a small phase delay between the droplet and local gas velocities of about 0.05π. As a first approximation, it is, therefore, possible to consider that the droplet velocities correspond to the air velocities at the injector outlet in the frequency range of interest.

3 DETERMINATION OF FLAME DESCRIBING FUNCTION (FDF)

Generally, in flames formed by a spray of fuel conveyed by a stream of air, one expects to find equivalence ratio fluctuations together with velocity fluctuations. One would have to determine two describing functions, one pertaining to equivalence ratio disturbances and the other to velocity or volume flow rate disturbances. One would write in general,

$$\dot{Q}'/\overline{\dot{Q}} = \mathcal{F}_\phi(\phi'/\overline{\phi}) + \mathcal{F}_v(\dot{q}_v'/\overline{\dot{q}_v}) \tag{1}$$

In the above equation, $\dot{q}_v$ is the volumetric flow rate, $\dot{Q}$ represents the HRR, $(\cdot)$' refers to fluctuations, and $\overline{(\cdot)}$ refers to the mean of a quantity. The flame would then have to be treated as a multiple input single output (MISO) system. However, as mentioned in Section 2, the relative equivalence ratio disturbances are an order of magnitude smaller than the volume flow rate (or velocity) disturbances (*i.e.*, $\phi'/\overline{\phi} \ll \dot{q}_v'/\overline{\dot{q}_v}$). One may then only consider the effects of volume flow rate disturbances (as a SISO system) and focus on the determination of $\mathcal{F}_v$. This is admittedly an approximation, but it is applicable in a situation where the relative HRR fluctuations are essentially induced by relative flow rate or equivalently velocity disturbances in the present experiments.

The FDF $\mathcal{F}_v$ gives the nonlinear response of the flame to the incoming acoustic perturbation as shown in Eq. 2. In what follows, the subscript v is dropped and $\mathcal{F}$ is simply used to designate the FDF.

$$\mathcal{F}(\omega, \dot{q}_v') = \frac{\dot{Q}'/\overline{\dot{Q}}}{\dot{q}_v'/\overline{\dot{q}_v}} \tag{2}$$

where ω is the angular frequency. It is experimentally difficult to obtain a measure of flow rate fluctuations at the injector outlet, especially when there is a swirling flow with large shear zones. It is rather easier to measure the local velocity fluctuations instead by optical velocimetry techniques such as LDA or by hot wire anemometry. The FDF expression can then be rewritten as:

$$\mathcal{F}(\omega, |u_{c,r}'|) = \frac{\dot{Q}'/\overline{\dot{Q}}}{u_{c,r}'/\overline{u}_{c,r}} = G(\omega, |u_{c,r}'|) e^{i\varphi(\omega, |u_{c,r}'|)} \tag{3}$$

where, $G = |\mathcal{F}|$ and $\varphi = arg(\mathcal{F})$ represent the FDF gain and phase, and $u_{c,r}'$ is a reference acoustic velocity fluctuation determined at the base of the flame (subscript 'c' referring to the measurement in the chamber) at a certain distance r from the center of the injector and at a particular height h from the chamber backplane. Equations (2) and (3) are equivalent only if:

$$\dot{q}_v'/\overline{\dot{q}_v} = u_{c,r}'/\overline{u}_{c,r} \tag{4}$$

It is crucial that the velocity measurement at the injector outlet be obtained at a location where Eq. 4 is valid, and this has been carefully considered in a previous study by the same authors [30]. As the velocity measurements by LDA require optical access, they are obtained at $h = 2.5$ mm above the injector exit plane. It is also found in [30] that the radial position

r of the velocity measurement point that fulfills Eq. 4 corresponds to nearly the maximum of the mean axial velocity for the swirling injectors considered here. For swirlers 707 and 807, this radial location is at $r = 3.5\,\text{mm}$, and for swirlers 716 and 816, this is at $r = 4\,\text{mm}$. As shown in [30], the quality of the FDF determination is sensitive to the location where velocity fluctuations are being measured. Since the velocity at the injector outlet changes rapidly, even a small displacement with respect to the optimal point can significantly alter the equality in Eq. 4, thereby changing the determined FDF gain. One also finds that a shift of the measurement point is accompanied by a reduction in signal-to-noise ratio producing phase values that are less reliable. This can be controlled by examining the coherence function and requiring that it be greater than a certain threshold, as indicated at the end of this section.

The FDF measurements are performed by subjecting the flame to different levels of acoustic velocity fluctuations induced by the four driver units located at the bottom of the plenum. A wave generator produces sinusoidal signals with an amplitude V_0 (peak to peak) ranging from 0.5 V to 2.9 V in steps of 0.3 V, and a linear frequency sweep is performed from 250 Hz to 850 Hz for a time duration of 133 s at each amplitude level. Modulating the air flow with different amplifier voltages produces different velocity fluctuation levels at the injector exit. The processor of the PDA/LDA system simultaneously acquires the PM voltage while measuring the velocity. The signals are then interpolated and resampled to obtain the cross power spectral density between the relative HRR and velocity modulations. It is ensured that the number of droplets passing through the LDA measurement volume is high enough ($\approx 30\,\text{kHz}$) to have a sufficient sampling rate. The coherence between the input relative velocity disturbances and output relative HRR disturbances is calculated, and the corresponding data are retained only if this coherence $\gamma^2 = |S_{\dot{Q}'u'_{c,r}}|^2/(S_{\dot{Q}'\dot{Q}'}S_{u'_{c,r}u'_{c,r}})$ is greater than a certain threshold. The choice is made to use $\gamma^2 \geq 0.9$, ensuring a signal-to-noise ratio of at least 9.5 dB.

4 RESULTS AND DISCUSSION

It is interesting to first examine flame images recorded in TICCA-Spray and compare them with images obtained in SICCA-Spray to uncover differences in terms of flame shapes. This will help interpret the FDF measurements corresponding to the different swirlers that are first shown for TICCA-Spray and then compared with the FDFs determined in SICCA-Spray.

4.1 Flame images in TICCA-Spray and SICCA-Spray

The first three columns in Fig. 4 display the flame images of TICCA-Spray and SICCA-Spray formed by the different swirling injectors at the two operating points in the first three columns. These images are recorded by a Panasonic Lumix FZ38 digital camera under steady conditions, and the driver units at the bottom of the test rigs are inoperative while recording these images. The fourth column shows the evolution of intensity integrated over all vertical pixels corresponding to each horizontal coordinate in the flame zone normalized by its maximum value. The normalized intensity is obtained from the images captured by an intensified CCD camera (PI-MAX from Teledyne Princeton Instruments) equipped with a Nikon 105 mm UV lens and OH^* filter centered at 310 nm. The flames formed by 707 (with adjacent co- or counter-rotating neighbors) in TICCA-Spray are, in general, longer and narrower with negligible interaction between the adjacent flames. This is apparent from the intensity plots in Fig. 4 (m) and (n), where the integrated intensity between the flames is quite low.

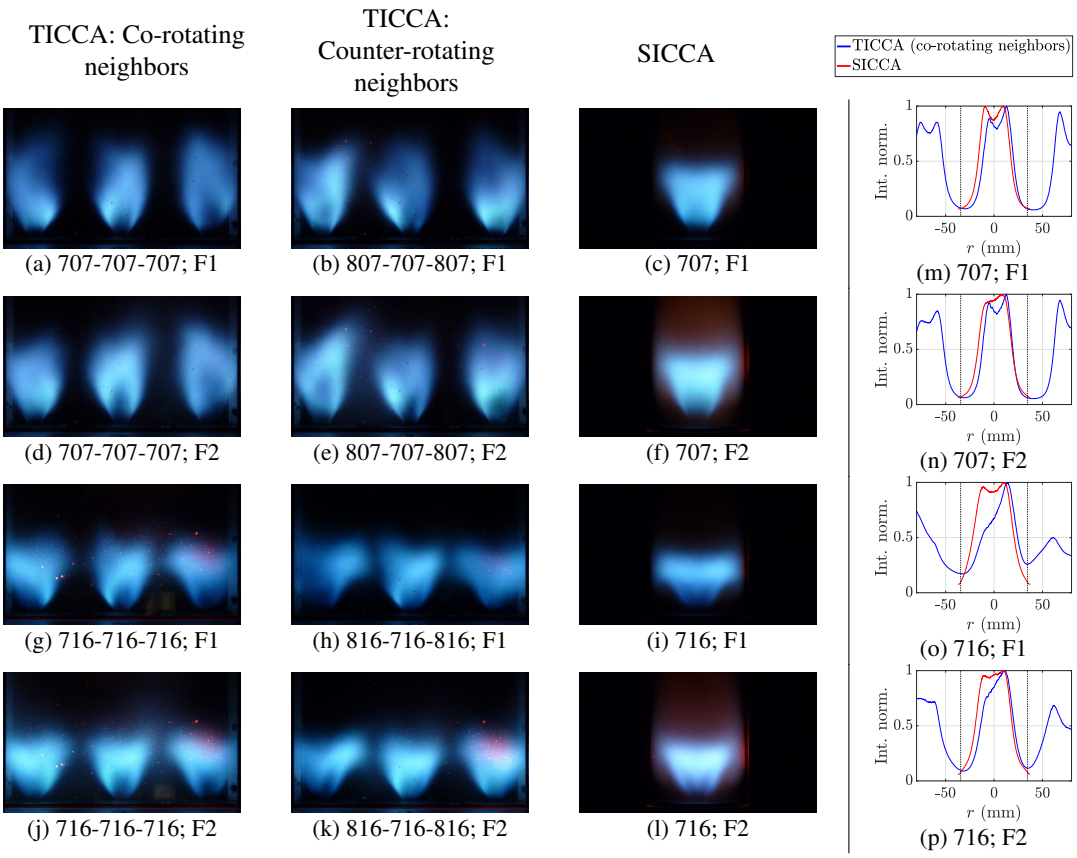

Fig. 4: Flame images in TICCA-Spray (first and second column) and SICCA-Spray (third column). In the first column the neighboring injectors are co-rotating, while in the second column, the neighboring injectors are counter-rotating. Images are adjusted to have the same aspect ratio and scale. The fourth column shows the evolution of intensity integrated over an ensemble of vertical pixels at each horizontal coordinate in the flame zone normalized by its maximum value. The blue lines correspond to TICCA-Spray with co-rotating neighbors and the red lines pertain to SICCA-Spray. Dotted black lines represent the chamber wall in SICCA-Spray. Here, the first and third rows correspond to the operating point F1, and the second and fourth rows correspond to F2.

Likewise, the flames of 707 in SICCA-Spray feature lesser interactions with the chamber walls but are comparatively shorter than in TICCA-Spray.

The flames established by 716 (with adjacent co- or counter-rotating neighbors) in TICCA-Spray are shorter and broader compared to 707, which results in augmented interaction with the neighboring flames. This can be notably seen at F1 in Fig. 4 (g) & (h), where the flame fronts touch their neighbors at the top. This is also apparent in the intensity plots in Fig. 4 (o) & (p), where the intensity level between flames is higher than for 707 (Fig. 4 (m) & (n)). The integrated intensity plots also indicate that the flames of 716 are broader than those of 707 in SICCA-Spray, indicating a higher flame-wall interaction with 716. The central flame of 716 is also less symmetric in TICCA-Spray (see Fig. 4 (o) & (p)), which could be due to the augmented interaction between flames and to the fact that all swirlers are co-rotating. At F2, the flames in TICCA-Spray are weakly interacting with the neighboring flames, and similarly, their interaction with the wall is reduced in SICCA-Spray. This is noticeable from Fig. 4 (p), where the intensity level between flames is lower in TICCA-Spray, and the flame is comparatively narrower in SICCA-Spray. With 716, the side flames of TICCA-Spray possess a shape similar to the wall-bounded flames of SICCA-Spray, which differs from the shape of the central flame in TICCA-Spray. The flames that

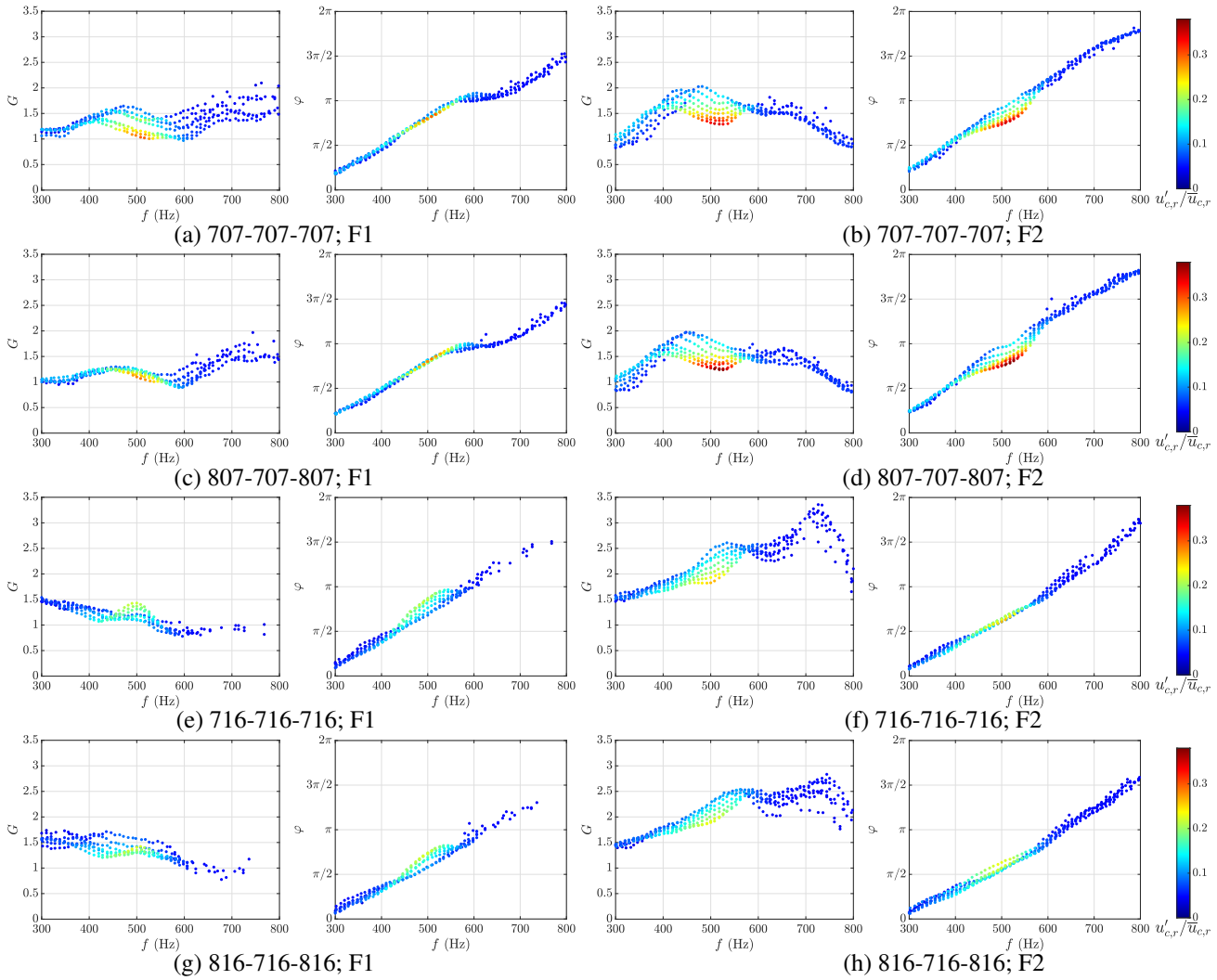

Fig. 5: Gain G and phase φ of FDFs measured in TICCA-Spray at the two operating conditions. The color scale represent the velocity fluctuation levels measured at the injector outlet.

interact with the wall feature wings on their sides that reach up to the lateral boundaries. The absence of this feature in the flames of 707 could be attributed to the reduced expansion of the flame and correspondingly reduced wall interaction. No obvious difference is visually observed in the flame images between co- and counter-rotating neighbors. For the two swirler arrangements, the flames at F2 are evidently brighter as they operate at a higher equivalence ratio. The general differences in the lateral extent of the flames between 707 and 716 may be linked to the higher swirl number of the latter, leading to a wider inner recirculation zone and an expanding flow field.

4.2 FDFs measured in the linear array facility TICCA-Spray

The FDFs measured in TICCA-Spray for the various swirlers and operating points are displayed in terms of gain G and phase φ in Fig. 5 for a range of frequencies and velocity fluctuation levels. Data are smoothed using a five-point moving average and shown only if the coherence between HRR and velocity signals is at least 0.90. Experiments have also been repeated to ensure that the data reported can be reproduced reasonably well. Substantial variations in the velocity fluctuation amplitudes are obtained up to 600 Hz, beyond which the system is only weakly responsive to acoustic perturbations. The

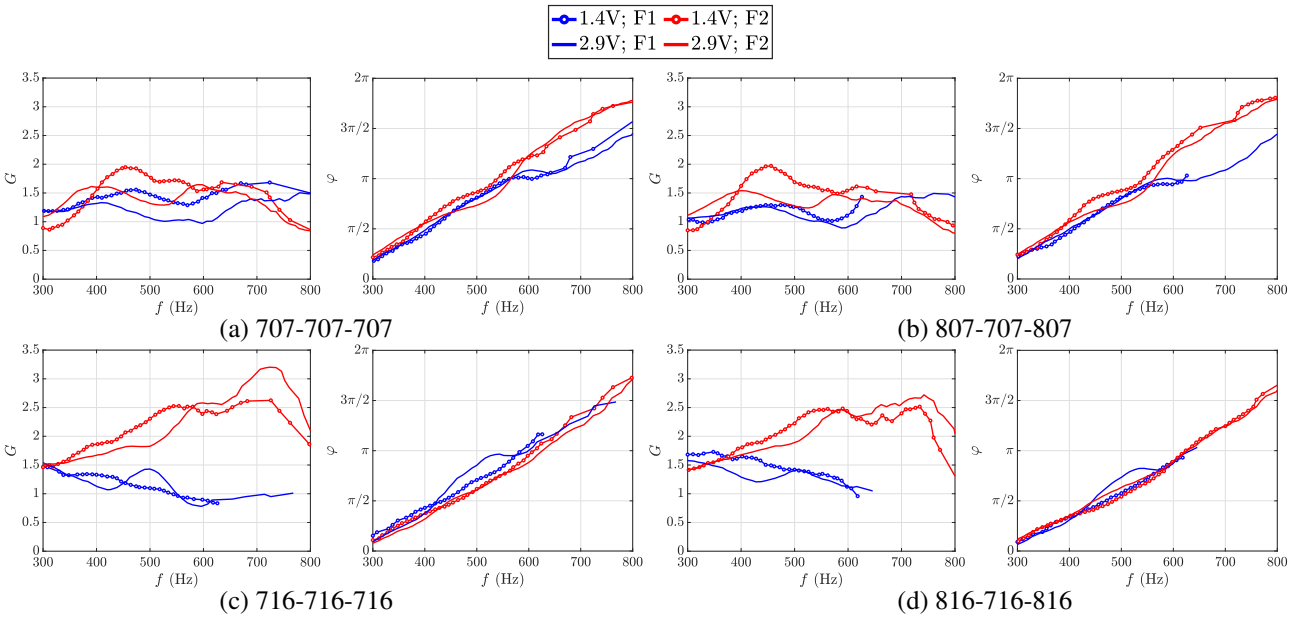

Fig. 6: Comparison between operating points: gain G and phase φ of the FDFs measured in TICCA-Spray showing comparison between the two operating points for the different swirler combinations (F1: blue, F2: red). Results are only plotted at two amplifier voltages $V_0 = 1.4\,\mathrm{V}$ (solid line with marker) and 2.9 V (solid line without marker) to illustrate the differences.

modulation level remains relatively low ($\approx 5\%$) beyond 600 Hz, and the signal levels are quite weak to consider any variation in the FDF. It might still be possible to analyze the flame dynamics linearly (as FTF) in this range, but caution is to be taken as the measurement uncertainties are expected to be higher in this region due to the poor signal-to-noise ratio.

Nonlinearity, especially in the gain, is observed between 400 Hz and 600 Hz for all the operating conditions except for 707 with adjacent counter-rotating swirlers at F1 (Fig. 5 (c)). The phase, however, is mostly independent of fluctuation amplitude except for 707 at F2 (Fig. 5 (b) and (d)) and 716 at F1 (Fig. 5 (e) and (g)) in the vicinity of 500 Hz (with both co- and counter-rotating neighbors). The change in equivalence ratio affects the FDF gain and phase, as can be seen in Fig. 6. The results are presented only at two amplifier voltages for better clarity. The difference is comparatively modest in the gain of 707 with both adjacent co- and counter-rotating swirlers. This could be attributed to the absence of strong flame-flame interaction with this swirler. The phase evolution for 707 is nearly the same at F1 and F2 until 550 Hz, beyond which the phase at F1 shows a plateau before increasing again. For 716, increasing the equivalence ratio from F1 to F2 leads to an increased gain, and at 700 Hz, the gain at F2 is about three times that found at F1. This variation in gain could be caused by the higher flame-flame interaction at F1 compared to F2 (see Fig. 4 (o) & (p)). The phase evolution nevertheless remains the same.

4.3 Comparison of FDF between co- and counter-rotating swirl

The TICCA-Spray test rig allows examining the effect of having counter-swirling flames next to the central flame rotating in the clockwise direction. Obviously, this effect cannot be examined in a single-injector configuration. Figure 7 shows, on the same graphs, the comparison of FDFs plotted in terms of amplifier voltages for the two swirler units and operating points when having adjacent co- or counter-swirling flames. Although a representation in terms of amplifier

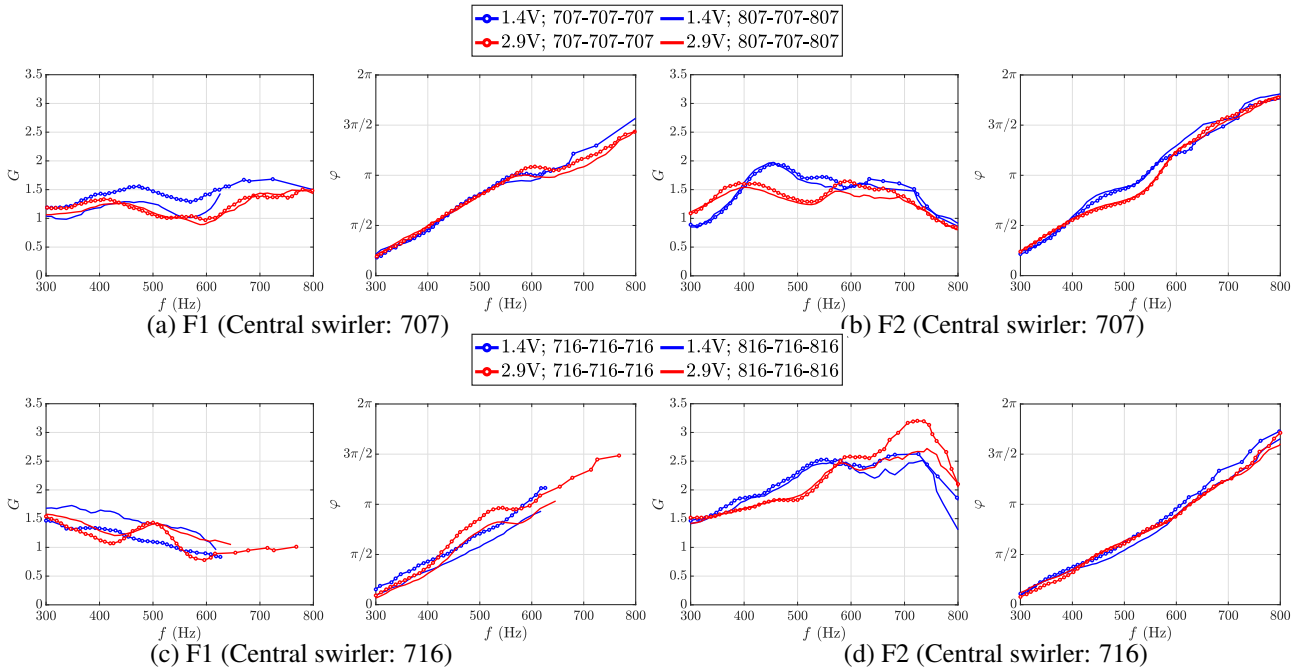

(a) F1 (Central swirler: 707) (b) F2 (Central swirler: 707)

(c) F1 (Central swirler: 716) (d) F2 (Central swirler: 716)

Fig. 7: Influence of neighboring swirlers: gain G and phase φ of the FDF measured in TICCA-Spray with co- (solid lines with marker) and counter-swirl (solid lines without marker) swirler combinations at the two operating points F1 and F2. Results are presented for two amplifier voltage $V_0 = 1.4\,\mathrm{V}$ and $2.9\,\mathrm{V}$ of the driver units.

voltage is not physically intuitive, it is reminded that they, in turn, are linked to velocity modulation level. To read these values, one could refer to Fig. 5.

Overall, the FDF of 707 does not depend on the type of the adjacent swirlers. Both gain and phase generally remain the same with both co- and counter-rotating swirlers, except for a minor difference in gain at $V_0 = 1.4\,\mathrm{V}$. On the contrary, the FDF of 716 has a higher dependence on the neighboring flames, especially at F1. Both the FDF gain and phase moderately differ depending on whether the adjacent swirlers are of 716 or 816 type. The gain with counter-rotating neighbors is slightly higher than that determined in the co-rotating case, whereas the phase takes slightly higher values with co-rotating swirlers. On the other hand, the difference in the FDF of 716 between co- and counter-rotating swirlers is only modest at F2, with minor variations in gain beyond 600 Hz. However, in this region, the velocity fluctuation level is relatively low (refer to Fig. 5 (f) & (h)) to reasonably identify a difference.

The reason for this variation in the dynamic response of the flame depending on the adjacent swirlers can be well understood from the flame images shown in Section 4.1. Flames with 707 are narrower and have visibly weaker interactions with adjacent flames. Thus, the FDF of 707 is influenced to a lesser extent by the presence of a co- or counter-rotating neighbor. In contrast, 716 flames are wider, and the span of the neighboring flames evidently extends to the central flame, resulting in stronger interactions with the neighbors. This interaction is more pronounced at F1, as seen from Fig. 4 (g) & (h), where the wings of the neighbors touch the central flame (also seen in (o)). This is manifested in the FDF as a strong variation in gain and phase between co- and counter-swirling flames. However, at F2, the flame is comparatively narrower, and its interaction with the side flames is weaker, resulting in similar FDF evolution in configurations where the central flame that rotates in the clockwise direction is surrounded by counterclockwise neighbors.

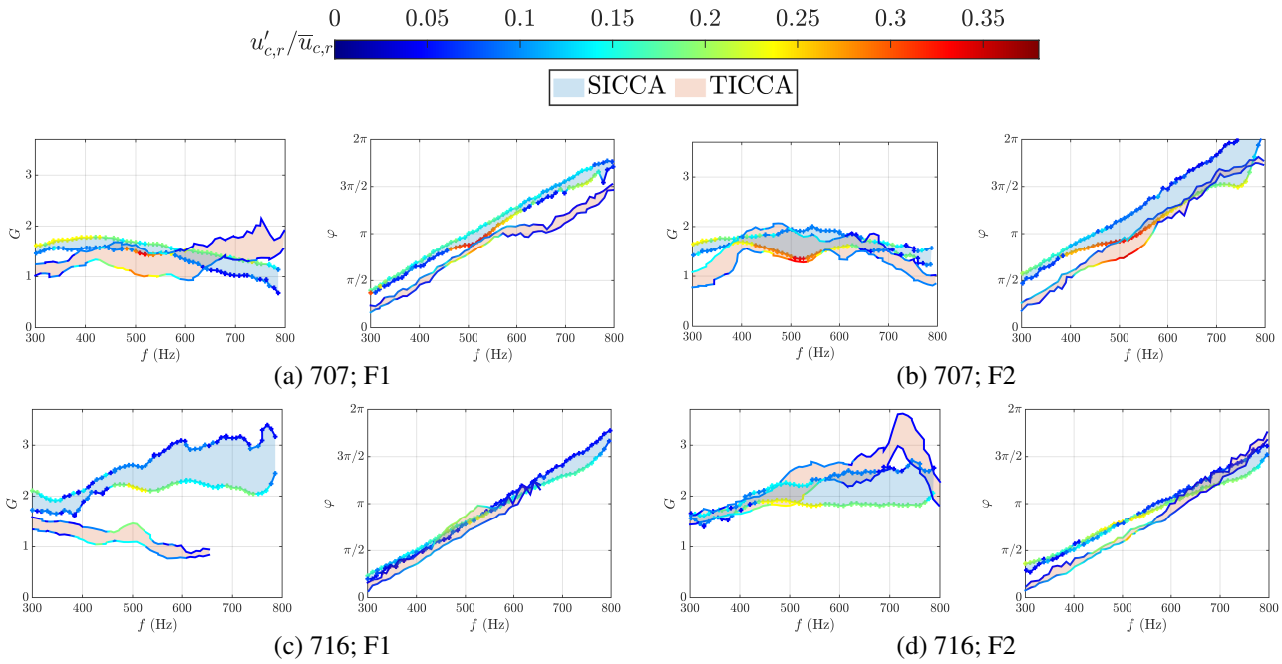

Fig. 8: Comparison of gain G and phase φ of the FDFs measured in the multiple-injector setup TICCA-Spray (solid lines without marker) with co-rotating neighbors and in the single-injector system SICCA-Spray (solid lines with marker) at the two operating points F1 and F2, and for the swirlers 707 and 716. The levels of velocity fluctuations $u'_{c,r}/\overline{u}_{c,r}$ are indicated by the color levels and the span of the FDF data is represented by the colored bands.

5 COMPARISON OF FDF MEASURED IN TICCA-SPRAY AND SICCA-SPRAY

This section compares the FDF measured in the three-injector test rig TICCA-Spray against the measurements from the single-injector test rig SICCA-Spray. The results of FDF in SICCA-Spray have been previously presented in [30]. This comparison will identify the adequacy of the widely used procedure of obtaining the FDFs from a single-injector test rig, an approach that is used, for example, in [28] to explain observed instabilities. The comparison of the FDFs pertains to the central swirler in TICCA-Spray when the adjacent flames are of co-rotating type. Figure 8 shows the FDF in terms of gain and phase between the two configurations. The FDFs obtained in SICCA-Spray are represented as solid lines with markers, and the FDF determined in TICCA-Spray is represented by solid lines without markers. These lines are colored according to the velocity fluctuation levels. The span of the FDF data obtained is represented by the colored bands, and the statistical uncertainties calculated by a bootstrapping method remain within this span. The levels of velocity fluctuations between the two systems match in the range from 300 Hz to 600 Hz. Beyond 600 Hz, the signal level in TICCA-Spray is too weak, and the coherence between the input velocity and the output heat release rate modulations is low, unlike in SICCA-Spray. At F1, a difference in gain exists for both swirlers; while this difference is modest for 707, the gain of 716 is significantly higher in SICCA-Spray than in TICCA-Spray. The reason for the higher gain in SICCA-Spray could be attributed to the flame-wall interaction illustrated in Fig. 4 (i) & (o). Such interactions induce strong variations in the flame surface area, which in turn contribute to sound production, as shown by Candel *et al.* [33]. At a higher equivalence ratio, the flame of swirler 716 is narrower and features reduced interaction with the chamber walls in SICCA-Spray and adjacent flames in TICCA-Spray, possibly explaining similar gain values between the two systems at F2. The gain of 707 at F2 is nearly the same between the two systems except for some minor differences at low frequencies.

On comparing the phase curves, one observes that the phase of 707 takes lower values in TICCA-Spray than in SICCA-Spray but evolves in a nearly similar fashion for both operating points. The dependence of the phase on the input velocity fluctuation level is prominent for swirler 707 at F2. One also notices a deviation in phase beyond 550 Hz at F1, but the velocity fluctuation levels are much lower in this zone for TICCA-Spray than SICCA-Spray. With 716, the phase takes the same values between TICCA-Spray and SICCA-Spray at F1, thereby indicating similar values for the time delay between velocity and HRR fluctuations. On the other hand, the phase for the swirler 716 at F2 has a different behavior than at F1; although it has a similar evolution, the phase value measured with TICCA-Spray is lower than that measured with SICCA-Spray below 600 Hz. This means that the time taken for the velocity fluctuations produced at the injector exit to reach the entire flame area will be the same between the two systems at F1, except that the phase is shifted by a constant value, unlike at F1. The behavior at F2 is similar to the observations with swirler 707 but different from the behavior of swirler 716 at F1. Further diagnostics of the flow and flame behavior would be necessary to explain the observed differences.

The differences in FDF between the two systems can be appreciated by considering their impact on instability prediction using low-order modeling such as the one proposed in [30] for injectors that are weakly transparent to acoustic waves or [13] for acoustically transparent injectors. As shown in the above works, the phase of the FDF often determines whether or not the system falls within an "unstable band" which can serve to predict a potential instability in a particular frequency range. Furthermore, the gain of the FDF determines the growth rate, which relates to the amplitude of instability, provided the growth rate is originally higher than the damping rate imposed by the system. This indicates that, for swirler 707, one could reasonably obtain similar growth rates irrespective of whether the FDF is measured with an isolated flame or in an environment where the flame is surrounded by adjacent neighbors. Regarding the phase, it was shown that, despite having similar slopes, it takes lower values in TICCA-Spray than in SICCA-Spray. This introduces some uncertainty in the prediction of potential instability. The phase curves in Fig. 8 (a) and (b) indicate a horizontal shift between the curves. This induces a 50 Hz displacement of the crossing point of the phase with one of the boundaries of the unstable region, causing a 50 Hz uncertainty on the range of frequencies where the instability might occur. Regarding swirler 716, the phase curves nearly coincide at F1, and the frequency range of potential instability can be assessed with smaller uncertainty. However, the differences in the FDF gains measured in SICCA-Spray and TICCA-Spray will give rise to notable changes in the growth rates. At F2, the differences observed in the FDF phase will result in some uncertainty in the frequency range of potential instability. Since the FDF gains are quite similar at F2 this will give rise to similar growth rates.

The above results indicate a moderate but non-negligible difference in the FDF between the two combustors. Also, whether the FDF measurement should be done in an isolated flame or a flame surrounded by the neighboring flames cannot be universally decided but rather depends on the flame geometry. In general, one would obtain an approximate prediction of the instability of an annular combustor using the FDF measured in a single-injector combustor if the flame-wall interaction is not too strong and provided that the backplane area is equivalent to that of a single sector of the annular combustor, *i.e.*, the area ratio A_I/A_{BP} is maintained. If A_I/A_{BP} is not conserved, the single-injector combustor will feature a different flow pattern, as can be seen in [26]. Nonetheless, a multi-injector system reflecting the flame-flame interaction found in the annular combustor would be worthwhile to get an accurate FDF and more precisely predict the instabilities. Since interactions

between injector flows are mainly governed by the flame geometry, the results presented here, although demonstrated on a spray combustor, can be expected to be applicable to premixed injectors as well.

6 CONCLUSION

This article primarily reports flame describing functions (FDFs) measurements on a newly-developed three-injector linear test rig. In a first-of-its-kind study, FDFs measured in an isolated flame formed by a confined single-injector combustor are compared to those corresponding to a flame surrounded by neighboring side flames to identify the effect of lateral boundary conditions. Measurements of FDFs are carried out with two swirlers varying in swirl intensity at two operating points differing in global equivalence ratio. The three-injector configuration allows to additionally study the effect of neighboring swirl direction on the FDF by placing either co- or counter-rotating swirlers in the lateral injectors.

Comparisons of FDFs measured in the single-injector SICCA-Spray and in the linear array TICCA-Spray reveal differences in gain and phase at a level that depends on the operating conditions. In general, larger differences arise in the gain in cases where flame-wall interactions are strong. In other cases where flame front interactions with lateral boundaries are less pronounced, the FDF gain remains almost the same between the two configurations. The phase curve corresponding to the multiple-injector situation features the same slope but exhibits an offset with respect to that determined in the single-injector system. This will have a moderate but non-negligible impact on predictions of instabilities based on FDFs measured in a single-injector combustor. The direction of rotation of the adjacent swirlers becomes particularly important when the flame fronts have pronounced interaction with their neighbors. If such interactions are negligible, the FDF is nearly the same with co- or counter-rotating neighbors.

The experiments reported here at eight operating conditions indicate that the decision on the suitability of measuring the FDF in an isolated flame or in an environment where a flame is surrounded by adjacent side flames has no single answer but rather depends on the flame geometry produced by the injector. In general, the FDFs measured with a single-injector combustor would approximately represent a multi-flame system if the flame-wall/flame-flame interaction is minor. In this case, an order-of-magnitude prediction of instability in an annular combustor can be obtained using the FDFs measured in a single-injector combustor, provided that the single-injector combustor possesses the same area as the single sector of the annular combustor. A multi-injector system will still be needed if one requires a more precise FDF measurement.

Acknowledgements

This work was supported by project FASMIC ANR16-CE22-0013 of the French National Research Agency (ANR) and by the European Union's Horizon 2020 research and innovation programme, Annulight with grant agreement no. 765998. The authors thank the reviewers for their helpful comments.

References

[1] Poinsot, T., 2017. "Prediction and control of combustion instabilities in real engines". *Proc. Combust. Inst.,* ***36***(1), pp. 1–28.

[2] Kunze, K., Hirsch, C., and Sattelmayer, T., 2004. "Transfer function measurements on a swirl stabilized premix burner in an annular combustion chamber". In Proc. ASME Turbo Expo 2004, no. GT2004-53106.

[3] Krebs, W., Flohr, P., Prade, B., and Hoffmann, S., 2002. "Thermoacoustic stability chart for high-intensity gas turbine combustion systems". *Combust. Sci. Technol.,* ***174***, pp. 99–128.

[4] Staffelbach, G., Gicquel, L. Y. M., Boudier, G., and Poinsot, T., 2009. "Large Eddy Simulation of self excited azimuthal modes in annular combustors". *Proc. Combust. Inst.,* ***32***, pp. 2909–2916.

[5] Bourgouin, J.-F., Durox, D., Moeck, J., Schuller, T., and Candel, S., 2013. "Self-sustained instabilities in an annular combustor coupled by azimuthal acoustic modes". In Proc. ASME Turbo Expo 2013, no. GT2013-95010.

[6] Worth, N. A., and Dawson, J. R., 2013. "Modal dynamics of self-excited azimuthal instabilities in an annular combustion chamber". *Combust. Flame,* ***160***(11), pp. 2476–2489.

[7] Dawson, J. R., and Worth, N. A., 2014. "Flame dynamics and unsteady heat release rate of self-excited azimuthal modes in an annular combustor". *Combust. Flame,* ***161***(10), pp. 2565–2578.

[8] O'Connor, J., Acharya, V., and Lieuwen, T., 2015. "Transverse combustion instabilities: Acoustic, fluid mechanic, and flame processes". *Prog. Energy Combust. Sci.,* ***49***, pp. 1–39.

[9] Prieur, K., Durox, D., Schuller, T., and Candel, S., 2017. "A hysteresis phenomenon leading to spinning or standing azimuthal instabilities in an annular combustor". *Combust. Flame,* ***175***, pp. 283–291.

[10] Prieur, K., Durox, D., Schuller, S., and Candel, S., 2018. "Strong azimuthal combustion instabilities in a spray annular chamber with intermittent partial blow-off". *J. Eng. Gas Turb. Power,* ***140***(3), p. 031503.

[11] Wolf, P., Staffelbach, G., Gicquel, L., Müller, J.-D., and Poinsot, T., 2012. "Acoustic and large eddy simulation studies of azimuthal modes in annular combustion chambers". *Combust. Flame,* ***159***(11), pp. 3398–3413.

[12] Laera, D., Schuller, T., Prieur, K., Durox, D., Camporeale, S. M., and Candel, S., 2017. "Flame describing function analysis of spinning and standing modes in an annular combustor and comparison with experiments". *Combust. Flame,* ***184***, pp. 136–152.

[13] Schuller, T., Poinsot, T., and Candel, S., 2020. "Dynamics and control of premixed combustion systems based on flame transfer and describing functions". *J. Fluid Mech.,* ***894***.

[14] Noiray, N., Durox, D., Schuller, T., and Candel, S., 2008. "A unified framework for nonlinear combustion instability analysis based on the describing function". *J. Fluid Mech.,* ***615***, pp. 139–167.

[15] Worth, N. A., and Dawson, J. R., 2019. "Characterisation of flame surface annihilation events in self excited interacting flames". *Combust. Flame,* ***199***, pp. 338–351.

[16] Durox, D., Prieur, K., Schuller, T., and Candel, S., 2016. "Different flame patterns linked with swirling injector interactions in an annular combustor". *J. Eng. Gas Turb. Power,* ***138***(10), p. 101504.

[17] Dolan, B., Gomez, R. V., and Gutmark, E., 2017. "Parametric study of alternating flow patterns in non-reacting

multiple-swirl flows". In 55th AIAA Aerospace Sci. Meet., no. AIAA 2017-1956.

[18] Kao, Y.-H., Tambe, S., and Jeng, S.-M., 2014. "Aerodynamics study of a linearly-arranged 5-swirler array". In Proc. ASME Turbo Expo 2014, no. GT2014-25094.

[19] Kao, Y.-H., Denton, M., Wang, X., Jeng, S.-M., and Lai, M.-C., 2015. "Experimental spray structure and combustion of a linearly arranged 5-swirler array". In Proc. ASME Turbo Expo 2015, no. GT2015-42509.

[20] Dolan, B., Gomez, R. V., and Gutmark, E., 2015. "Optical measurements of interacting lean direct injection fuel nozzles with varying spacing". In Proc. ASME Turbo Expo 2015, no. GT2015-43706.

[21] Worth, N. A., and Dawson, J. R., 2012. "Cinematographic OH-PLIF measurements of two interacting turbulent premixed flames with and without acoustic forcing". *Combust. Flame,* ***159***(3), pp. 1109–1126.

[22] Lee, T., Lee, J., Park, J., Han, D., and Kim, K. T., 2018. "Staggered swirler arrangement in two self-excited interacting swirl flames". *Combust. Flame,* ***198***, pp. 363–375.

[23] Lee, T., Park, J., Han, D., and Kim, K., 2019. "The dynamics of multiple interacting swirl-stabilized flames in a lean-premixed gas turbine combustor". *Proc. Combust. Inst.,* ***37***(4), pp. 5137–5145.

[24] Ciardiello, R., Pathania, R. S., El Helou, I., and Mastorakos, E., 2021. "Lean blow-off investigation in a linear multi-burner combustor operated in premixed and non-premixed modes". *Appl. Energy Combust. Sci.,* ***9***, p. 100041.

[25] Fanaca, D., Alemela, P. R., Ettner, F., Hirsch, C., Sattelmayer, T., and Schuermans, B., 2008. "Determination and comparison of the dynamic characteristic of a perfectly premixed flame in both single and annular combustion chambers". In Proc. ASME Turbo Expo 2008, no. GT2008-50781.

[26] Fanaca, D., Alemela, P. R., Hirsch, C., and Sattelmayer, T., 2010. "Comparison of the Flow Field of a Swirl Stabilized Premixed Burner in a Annular and a Single Burner Combustion Chamber". *J. Eng. Gas Turb. Power,* ***132***(7).

[27] Smith, T., Chterev, I., Emerson, B., Noble, D., and Lieuwen, T., 2018. "Comparison of single- and multinozzle reacting swirl flow dynamics". *J. Propul. Power,* ***34***(2), pp. 384–394.

[28] Rajendram Soundararajan, P., Vignat, G., Durox, D., Renaud, A., and Candel, S., 2021. "Effect of different fuels on combustion instabilities in an annular combustor". *J. Eng. Gas Turb. Power,* ***143***(3), p. 031007.

[29] Vignat, G., Durox, D., Renaud, A., and Candel, S., 2020. "High amplitude combustion instabilities in an annular combustor inducing pressure field deformation and flame blow off". *J. Eng. Gas Turb. Power,* ***142***(1), p. 011016.

[30] Rajendram Soundararajan, P., Durox, D., Renaud, A., Vignat, G., and Candel, S., 2022. "Swirler effects on combustion instabilities analyzed with measured FDFs, injector impedances, and damping rates". *Combust. Flame,* ***238***(4), p. 111947.

[31] Hurle, I. R., Price, R. B., Sugden, T. M., and Thomas, A., 1968. "Sound emission from open turbulent premixed flames". *Proc. R. Soc. London Series A-Math. Phys. Sci.,* ***303***(1475), pp. 409–427.

[32] Ballester, J., and García-Armingol, T., 2010. "Diagnostic techniques for the monitoring and control of practical flames". *Prog. Energy Combust. Sci.,* ***36***(4), pp. 375 – 411.

[33] Candel, S., Durox, D., and Schuller, T., 2004. "Flame interactions as a source of noise and combustion instabilities". In 10th AIAA/CEAS Aeroacoust. Conf., p. 2928.